Boron and nitrogen co-doped sodium alginate-based porous carbons for durable and fast Zn-ion hybrid capacitors

LU Ya-ping[1,†], WANG Hong-xing[1,†], LIU Lan-tao[1,2], PANG Wei-wei[2], CHEN Xiao-hong[1,*]

（1. *State Key Laboratory of Chemical Resource Engineering*, *Beijing Key Laboratory of Electrochemical Process and Technology for Materials*, *Beijing University of Chemical Technology*, *Beijing* 100029, *China*;
2. *Petrochemical Research Institute*, *PetroChina Company Limited*, 102206 *Beijing*, *China*）

Abstract: In recent years, zinc-ion hybrid capacitors (ZIHCs) have attracted increasing attention due to their environmental friendliness and excellent electrochemical properties. However, their performance is mainly limited by the electrochemical performance of the cathode, so it is necessary to develop an advanced cathode material. N, B co-doped sodium alginate-based porous carbon (NBSPC) was prepared by one-step co-carbonization using sodium alginate as the matrix and $NH_4B_5O_8$ as the N and B source. This N, B co-doping strategy improves the pore structure of the carbon materials and increases the number of surface functional groups, greatly improving the capacitive behavior of the raw materials and thus improving their electrochemical performance. When used as the cathode in ZIHCs, the NBSPC had an excellent rate performance (85.4 mA h g^{-1} even at ultra-high current density of 40 A g^{-1}) and good cycling stability (15 000 cycles at 20 A g^{-1} with a capacity retention rate of 94.5%).

Key words: Sodium alginate-based porous carbon; N, B co-doped; One step hydrothermal activation; Zinc-ion hybrid capacitors

1 Introduction

In the past two decades, energy storage technology has developed rapidly, resulting in the increasingly excellent performance of electric vehicles and portable mobile devices [1–3]. This is all due to the rapid development of batteries and supercapacitors. Among numerous electrochemical energy storage devices (EESDs), lithium-ion batteries (LIBs) have occupied most of the commercial market owing to their superior energy density[4–6]. However, the lack of lithium resources, safety issues of organic electrolytes and environmental pollution limit the further development of LIBs[7–10]. Therefore, it is necessary to develop a novel high-performance aqueous electrolyte EESD. As an emerging EESD with aqueous electrolyte, Zn-ion hybrid capacitor (ZIHC) has higher energy density and similar power density compared to aqueous supercapacitors. Thus, it has attracted many scholars to conduct research in recent years.

In terms of device structure, a typical ZIHC is mainly composed of a zinc metal anode and an advanced material cathode[9,11]. Therefore, the performance of a ZIHC mainly depends on the performance of the cathode material[12]. Porous carbon is an ideal material for the ZIHC cathode because of the strong structural designability, low-cost and environmentally friendliness[13,14]. At present, high-quality porous carbon electrode materials can be prepared through both the hard template and soft template methods[15]. However, the complicated removal process of hard templates and the high price of soft template agents limit the large-scale preparation of porous carbons[16]. Consequently, it is imperative to explore a method for synthesize porous carbons without adding templates. In addition, modification of porous carbon materials is also a key step to improve their electrochemical performance in ZIHCs[17]. The more commonly used modification method is to introduce defects and active groups by doping heteroatoms into the carbon matrix to improve the zinc storage capacity and rate performance of porous carbons[18]. For instance, Chen et al. prepared a N-doped biomass porous carbon with one step carbonization, which exhibits 140 mAh g^{-1} at 0.2 A g^{-1} and 86.2 mAh g^{-1} at 6.4 A g^{-1} in a ZIHC[9]. Qiu et al. synthesized O, S co-doped porous carbon nanosheets, which shows a high capacity (194 mAh g^{-1}

Received date: 2024-01-26; **Revised date:** 2024-03-21

Corresponding author: CHEN Xiao-hong, Professor. E-mail: chenxh@mail.buct.edu.cn

Author introduction: †LU Ya-ping and WANG Hong-xing were contributed equally to this work

Supplementary data associated with this article can be found in the online version.

at 0.5 A g^{-1}) in ZIHC[19]. Yang and his co-workers developed a N/P co-doped hierarchical porous carbon for ZIHCs, which also exhibits good electrochemical performance[16]. There are many types of heteroatoms (such as N, S, O and B), and there are also some wonderful synergistic effects between different heteroatoms, which have a great impact on the zinc storage performance of carbon materials[20]. Therefore, it's necessary to develop a high-performance heteroatom-doped porous carbon.

In this work, the N, B co-doped sodium alginate-based porous carbons (NBSPCs) are prepared by one-step co-carbonization (Scheme 1). Due to the self-template of sodium alginate (SA)[2] and the large amount of gas generated by the decomposition of ammonium borate, NBSPCs have an improved hierarchical porous structure. In addition, this co-carbonization method can efficiently doped N and B into the carbon skeleton. This N, B co-doped strategy can improve the wettability and electric double layer electrochemical behavior of the materials. When used as the cathode in zinc-ion hybrid capacitor (ZIHCs), the optimized NBSPC shows excellent rate performance (85.4 mAh g^{-1} even at ultra-high current density of 40 A g^{-1}) and cycling stability (15 000 cycles at 20 A g^{-1} with a capacity retention rate of 94.5%). This efficient strategy provides a new idea for developing high-performance cathode materials for ZIHCs.

2 Experimental

2.1 Preparation of NBSPC-X

First of all, 2 g SA (AR, the average molecular mass of 12000-40000, purchase of purchased from Da Mao Chemical Reagent Factory in Tianjin) and different mass of $NH_4B_5O_8·4H_2O$ (3 g, 4 g, 5 g) were added into 140 mL deionized water in a beaker and stirred at room temperature overnight. The solution was then transferred into a Teflon sealed autoclave chamber for hydrothermal reaction at 160 °C for 12 h. After completely cooling in a refrigerator and freeze drying for 48 h, the target product, SA-derived carbon precursors, was obtained. Subsequently, the sample underwent additional pyrolysis in a tube furnace at 700 °C under N_2 protection, with a heating rate of 5 °C min^{-1} for 2 h. Then, in a tube furnace, under the protection of N_2 at 700 °C, further pyrolysis was conducted at a heating rate of 5 °C min^{-1} for 2 h. The products were washed by 1 mol L^{-1} HCl solution and deionized water to remove the templates. The final samples were denoted as NBSPC-X (nitrogen and boron co-doped SA derived porous carbon material), where X represented mass of $NH_4B_5O_8·4H_2O$.

2.2 Characterization

The structure of samples was tested by transmission electron microscopy (TEM, Hitachi 7700), scanning electron microscopy (SEM, ZEISS SUPRATM field emission microscopy) and high-resolution transmission electron microscopy (JEOL 3010, Japan). X-ray photoelectron spectra (XPS, ESCALAB250 electron spectrometer), X-ray diffraction (XRD, Rigaku D/max-2500B2+/PCX, Cu Ka), Raman spectroscopy (Aramis, Jobin Yvon, using 532 nm laser excitation) were used to study the composition of the material. The specific surface area and pore volume size were studied by N_2 adsorption–desorption (Micromeritics ASAP 2020), and calculated by density functional theory method and the Brunauer-Emmett-Teller model.

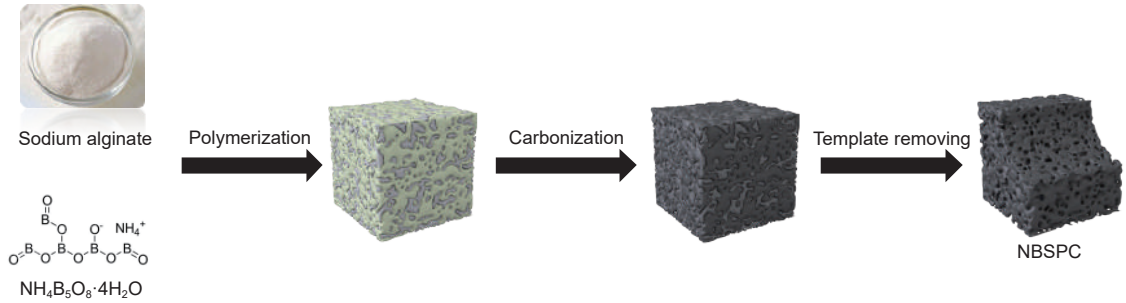

Scheme 1　An illustration of the preparation of NBSPC

2.3 Electrochemical measurements

The electrochemical performance of NBSPC-X was studied in symmetric two-electrode systems using 6 mol L^{-1} KOH (99.999%, purchased from Aladdin Industrial Corporation) electrolyte. The active material was mixed with acetylene black and polytetrafluorethylene (PTFE, purchased from Alading Industries) at a ratio of 8∶1∶1 on nickel foam to prepare the working electrode (the thickness of the active material was ≈ 0.026 mm), and the electrode was dried under vacuum at 120 °C for 12 h. The ZIHCs were prepared by zinc anode (7.14 g cm^{-3} of density and 80 mm of thickness) and NBSPC-X cathode in 2 mol L^{-1} $ZnSO_4$ electrolyte. The cathode was prepared by mixing NBSPC-X, acetylene black and polyvinylidene fluoride (PVDF)(≥98%, purchased from Aladdin Industrial Corporation) at a ratio of 8∶1∶1, uniformly coated on carbon cloth, and dried under vacuum at 120 °C for 12 h, with an area of 1.131 cm^{-2}. The surface mass load is about 1.0 ~ 1.3 mg cm^{-2}, and the total mass of active substances in the cathode is about 1.1 ~ 1.5 mg. All electrochemical tests are performed at the CHI660E Electrochemical workstation. CV curves are tested at scan rates ranging from 10 to 500 mV s^{-1}. Galvanostatic charge/discharge was performed from 0.2 to 50 A g^{-1}. The electrochemical impedance spectroscopy (EIS) was performed in the frequency ranging from 0.01 to 10 000 Hz with the amplitude of 5 mV.

3 Results and discussion

Fig. 1 shows the morphology of NBSPC-4. Figs. 1a-b shows that the NBSPC-4 has lamellar honeycomb porous structure. In Fig. S1, NBSPC with different ammonium borate dosages also exhibit obvious porous structures. The mechanism of this self-templated formation of porous carbon has been discussed in detail in previous work of our research group[2,3]. Fig. S1 shows the carbon matrix of NBSPC samples was severely etched, the pores collapsed, and the pore structure was mainly micropores. However, the carbon skeletons of samples doped with N and B atoms are stable, and most of them are mesoporous. As shown in Fig. 1c-e , many poles can be observed, indicating that this preparation strategy can effectively synthesize porous carbon. From the yellow circular marks in Fig. 1e, it can be seen that NBSPC-4 has a large number of mesoporous and macroporous surfaces, which is conducive to creating more diffusion channels to optimize ion transport, thus effectively improving the kinetic properties of carbon materials. Fig. 1f shows chaotic lattice stripes of NBSPC, which indicates NBSPC is a typical amorphous carbon structure. The illustration shows the carbon layer spacing obtained by Fourier transformation of lattice fringes is 0.45 nm, higher than the graphite carbon layer spacing of 0.335 nm, which is conducive to the embedding and removal of Zn^{2+}. Consistently, the ambiguous SEAD diffraction rings in Fig. 1g can also prove that NBSPC is amorphous carbon, the disordered structure can increase the pore space utilization of the electrode and improve the capacitive performance. The results of HAADF analysis and mapping test are shown in Fig. 1h-i. This result shows C, N, O and B are evenly distributed on the surface of NBSPC, indicating that this co-carbonization strategy successfully doped N and B elements into the sample.

As shown in Fig. 2a, there are obvious differences between the nitrogen adsorption-desorption curves of NBSPC and NBSPC-X. NBSPC shows typical type Ⅱ isotherms, indicating its pore structure is mainly composed of micropores, which mainly due to the SA-template pore-making mechanism. However, B, N co-doped samples exhibit type Ⅳ isotherms, indicating the coexistence of mesopores and micropores. Mesoporous pores contribute to the rapid diffusion of ions, and large pores can be used as ion buffer pools. Consistently, the pore size distribution shows the same results (Fig. 2b). The BET test shows that this B, N co-doping strategy reduce the specific surface area of the material (Table S1), and shows that there is a synergy between B atoms and N atoms. In the Raman spectrum of carbon materials, the ratio of I_D and I_G is usually used to measure the defect content of carbon materials[21]. In Fig. 2c, the ratio of I_D and I_G of NBCPS-4 is the largest compared to other samples.

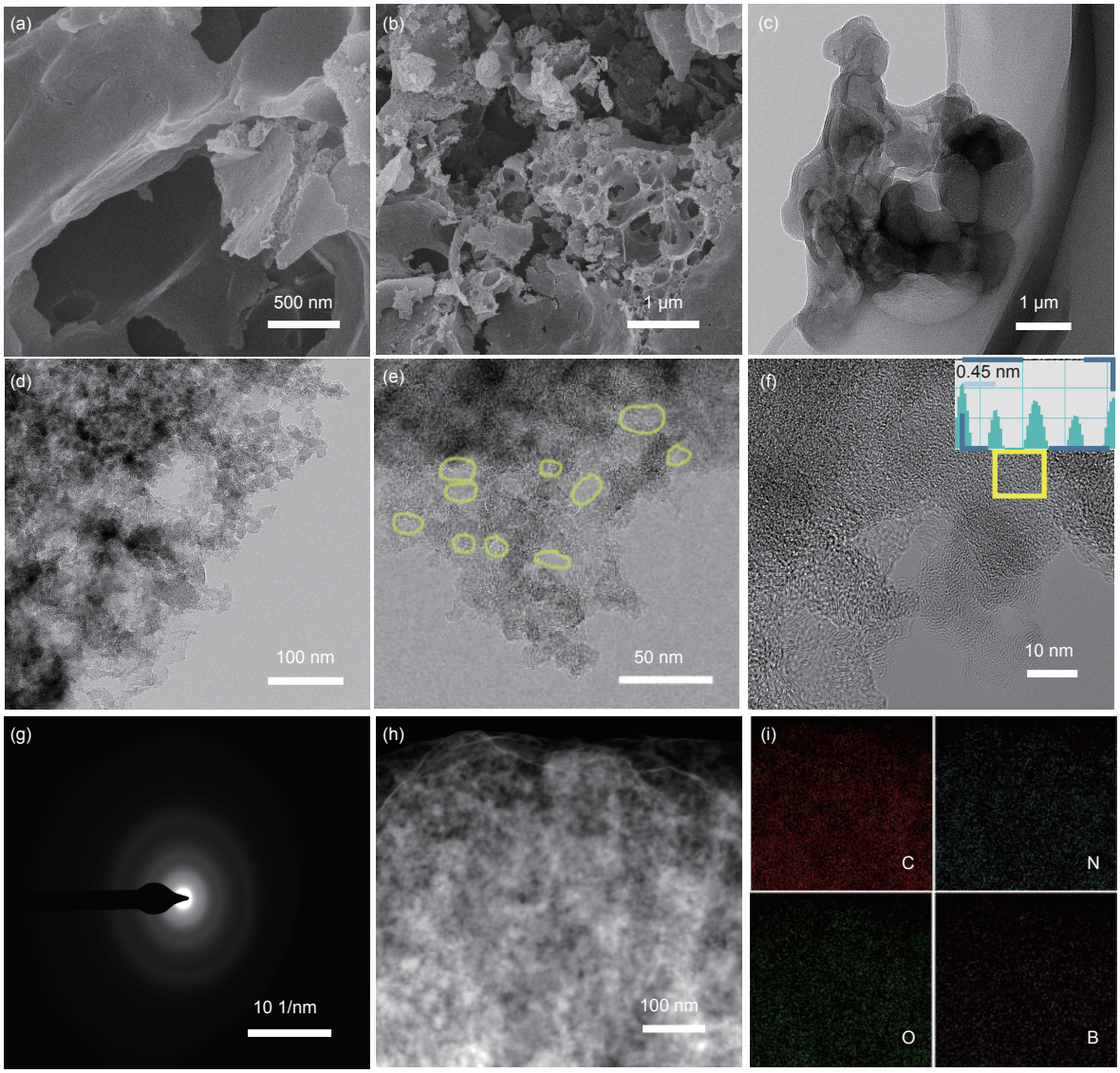

Fig. 1　(a-b) SEM images of NBSPC-4. (c-d) TEM images of NBSPC-4. (e-f) HRTEM images of NBSPC-4. (g) SAED patterns. (h-i) HAADF analysis and mapping

This result shows that as the B, N doping amount increases, the defects of the sample increase, but when the doping is excessive, the material defects begin to decrease again. XRD patterns shows the NBSPC and NBSPC-X are all amorphous carbon (Fig. 2d). In FTIR spectrum (Fig. 2e), diffraction peaks appear at 1 175 and 1 000 cm^{-1}, representing B—C and B—O bonds respectively, indicating the successful doping of B element[22]. Fig. 2f, Fig. S2 and Table S2 exhibit the results of XPS test. As shown in Fig. 2f and Table S2, as the amount of ammonium borate increases, the content of N and B elements increases. In addition, as shown in Fig. S2, there is a significant increase in C—N—B and C—B bonds. These results illustrate the successful doping of N and B elements[23]. The NBSPC-4 sample has a relatively high proportion of N-5 and N-6 atoms, both of which provide a higher electrochemical activity for the material. Compared to other samples, the NBSPC-4 sample contains the most C-N-B bonds (28.8%), which can optimize the unstable defects in the carbon network and promote the structural stability of the carbon material.

As shown in Fig. 3, the electrochemical performance of NBSPC and NBSPC-X as symmetric supercapacitor electrodes in 6 mol L^{-1} KOH were evaluated in detail. In Fig. 3a, NBSPC-4 exhibits the longest discharge time, suggesting that NBSPC-4 has the largest specific capacity[24]. Consistently, Fig. 3b shows that

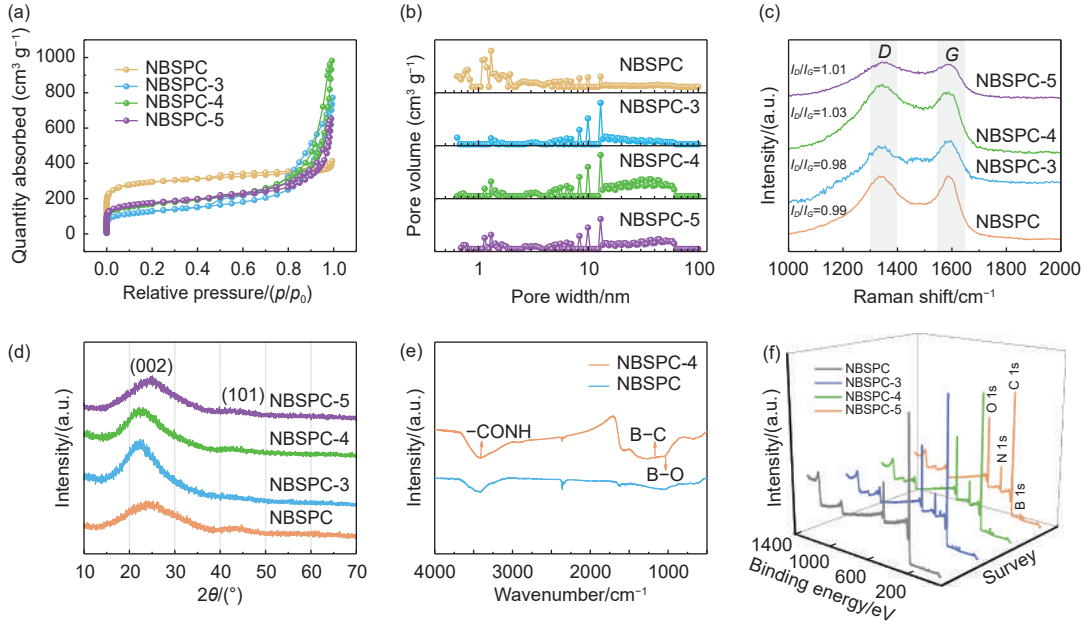

Fig. 2 Characterization of NBSPC samples: (a) Nitrogen adsorption-desorption curves. (b) Pore size distribution. (c) Raman spectroscopy. (d) XRD diffraction curves. (e) FTIR spectra. (f) XPS survey spectra

NBSPC-4 also has the largest CV pattern area, which also indicates that NBSPC-4 has the highest specific capacity. This result shows that compared with the undoped sample, the B, N functional groups provide ad-

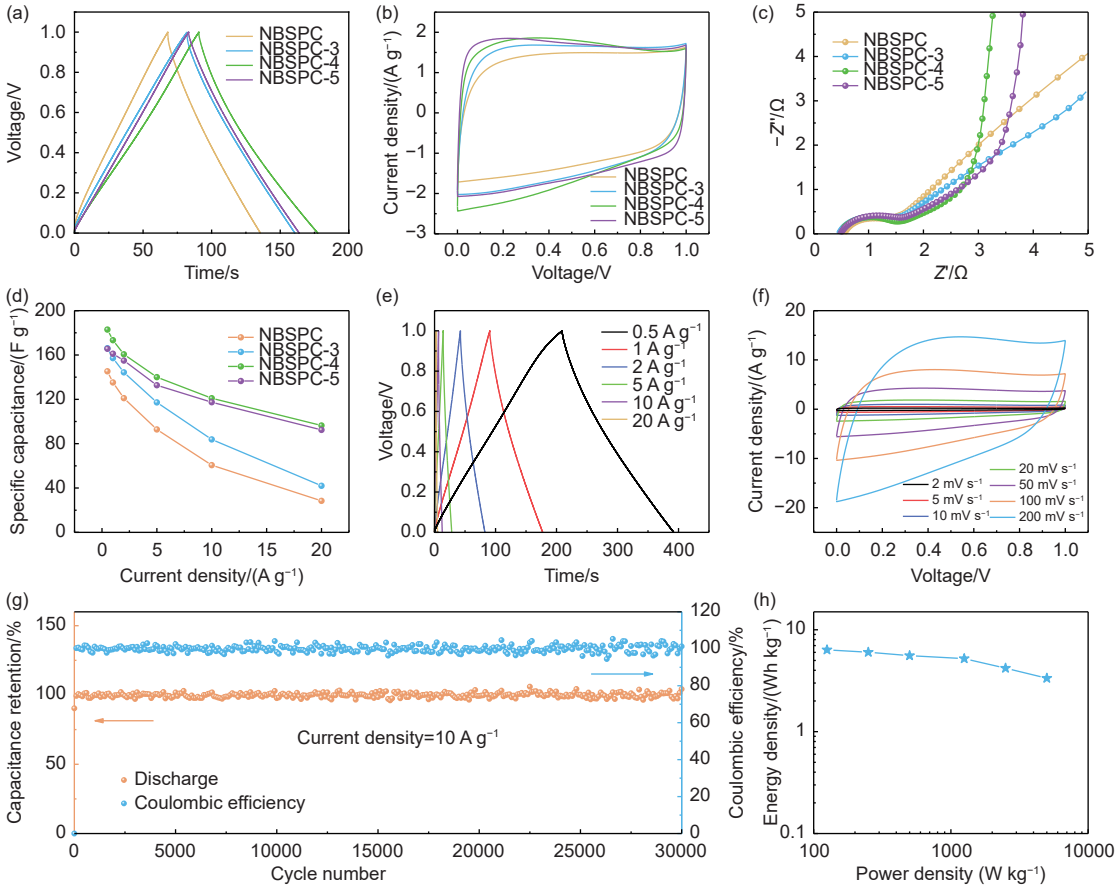

Fig. 3 Electrochemical performance of symmetric supercapacitor: (a) GCD curves. (b) CV curves. (c) Nyquist plots. (d) Specific capacitances at different current densities. (e) GCD curves of NBSPC-4 at different current densities. (f) CV curves of NBSPC-4 at different scan rates. (g) Cycling stability. (h) Energy density and power density

ditional pseudocapacitance to increase the specific capacity. However, excess B reduce the specific capacity because the excess B elements reduce the conductivity of the electrode[25]. As shown in Fig. 3c, NBSPC-4 exhibits the largest linear slope in the low frequency region, indicating the fastest diffusion behavior. This is because the B, N functional group improve the wettability of the material surface to the electrolyte. Fig. 3d shows that NBSPC-4 has the highest specific capacity and rate performance, which is also attributed to the above conclusions. As shown in Fig. 3e, NBSPC-4 exhibits an isosceles triangle-like shape under different current densities, indicating the energy storage mechanism of coexistence of pseudocapacitance and electric double layer capacitance. Fig. 3f shows that NBSPC-4 exhibits a quasi-rectangular shape at different scan rates, which also illustrates the coexistence mechanism of pseudocapacitanceandelectricdouble-layercapacitance[26].Asshownin Fig. 3g, NBSPC-4 demonstrates excellent cycle stability, and can be cycled stably for 30 000 times at 10 A g^{-1} with a capacity retention rate of 97.8%. The calculated energy and power density are shown in Fig. 3h, which is 6.35 Wh kg^{-1} (125 W kg^{-1}) and 3.35 Wh kg^{-1} (5 000 W kg^{-1}).

As shown in Fig. 4, NBSPC-4 exhibits excellent electrochemical performance of ZIHCs. ZIHCs are assembled with NBSPC as cathode and Zn metal as anode (Fig. 4a). As shown in Fig. 4b, NBSPC-4 exhibits the highest discharge time compared with other samples, which indicates the highest specific capacity[27]. It is proved that the synergistic effect of N and B co-doping plays an important role in capacity enhancement. Consistently, in Fig. 4c, NBSPC-4 has the largest CV curve area, which also shows that NBSPC-4 has the highest specific capacity. In addi-

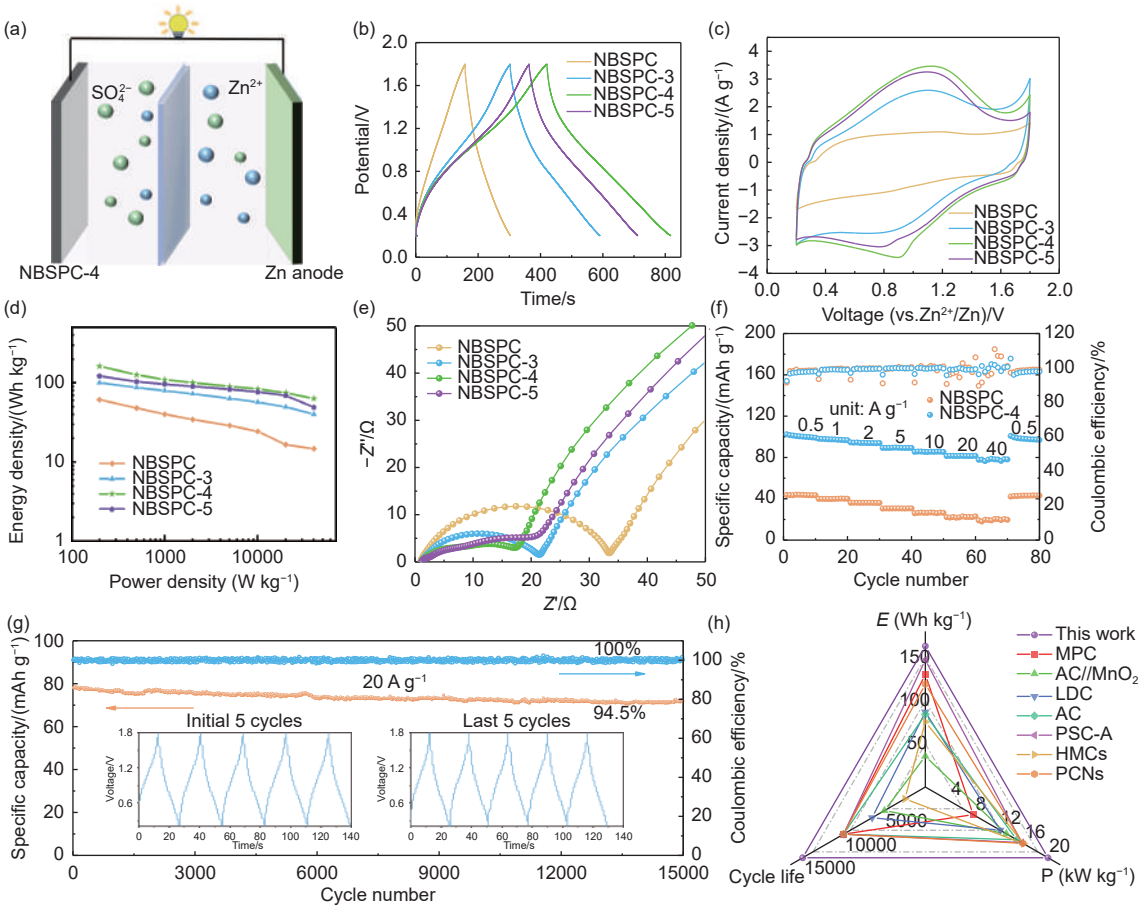

Fig. 4　Electrochemical performance of Zn-ion hybrid capacitor: (a) Schematic illustration of ZIHCs. (b) GCD curves. (c) CV curves. (d) Energy/power density comparison. (e) Nyquist plots. (f) Rate performance. (g) Cycling stability. (h) Comparison of energy density, power density, and cycling stability of NBSPC-4 and other types of advanced carbon materials

tion, the curves of NBSPC samples show a relatively regular quasi-rectangular shape, while the curves of doped samples show obvious hump and distortion, which is due to the redox reaction triggered by the inclusion of N and B heteroatoms. By calculation, NBSPC-4 delivers the highest energy density (Fig. 4d), which are 162.9, 127.1, 110.2, 100.7, 90.8, 83.9, 75.0, and 63.5 Wh kg^{-1} at 200, 500, 1 000, 2 000, 5 000, 10 000, 20 000 and 50 000 W kg^{-1}, respectively. As shown in Fig. 4e, NBSPC-4 has the smallest semicircle in the high frequency region and the straight line with the largest slope in the low frequency region, indicating that it has the smallest charge transfer resistance (R_{ct}) and the fastest diffusion behavior, which benefits from the reasonable pore structure and sufficient functional groups of NBSPC-4. Combining these advantages, NBSPC-4 shows a rate performance (Fig. 4f) of 102.4, 100.2, 97.5, 96.7, 94.1 and 85.4 mA h g^{-1} when the current densities are 0.5, 1, 2, 5, 10, 20 and 40 A g^{-1}, respectively, which far exceeds that of NBSPC. As shown in Fig. 4g, NBSPC-4 can stably cycle 15 000 times at an ultra-large current density of 20 A g^{-1} with a capacity retention rate of 94.5%. It is worth mentioning that the GCD curves in the first 5 cycles are almost the same as those in the last 5 cycles, which also shows the excellent stability of NBSPC-4[28]. In Fig. 4h, compared with other recently published ZIHCs cathode materials, NBSPC-4 is at a higher level in terms of energy density, power density and cycle life.

The kinetic analysis of NBSPC-4 is shown in Fig. 5. GCD tests with different current densities are used, as shown in Fig. 5a. The curve shows a similar quasi-triangular shape, indicating that the material has good reversibility and electrical conductivity[29]. The *b* values of the oxidation peak and the reduction peak are calculated from the CV curves at different scan speeds in Fig. 5b. The closer the *b* value is to 0.5, the electrochemical behavior is dominated by diffusion, and the closer the *b* value is to 1, the electrochemical behavior is dominated by capacitive behavior. As shown in Fig. 5c, the *b* values of both peaks are close to 1, which once again confirms that NBSPC-4 is dominated by capacitive behavior[30]. This is because the porous structure and abundant functional groups on the surface promote the material's adsorption behavior of Zn ions. The results of capacitive and diffusion-controlled contribution are exhibited in Fig. 5d and Fig. 5e. Consistent with the previous results, NBSPC-4 is mainly based on capacitive behavior. As

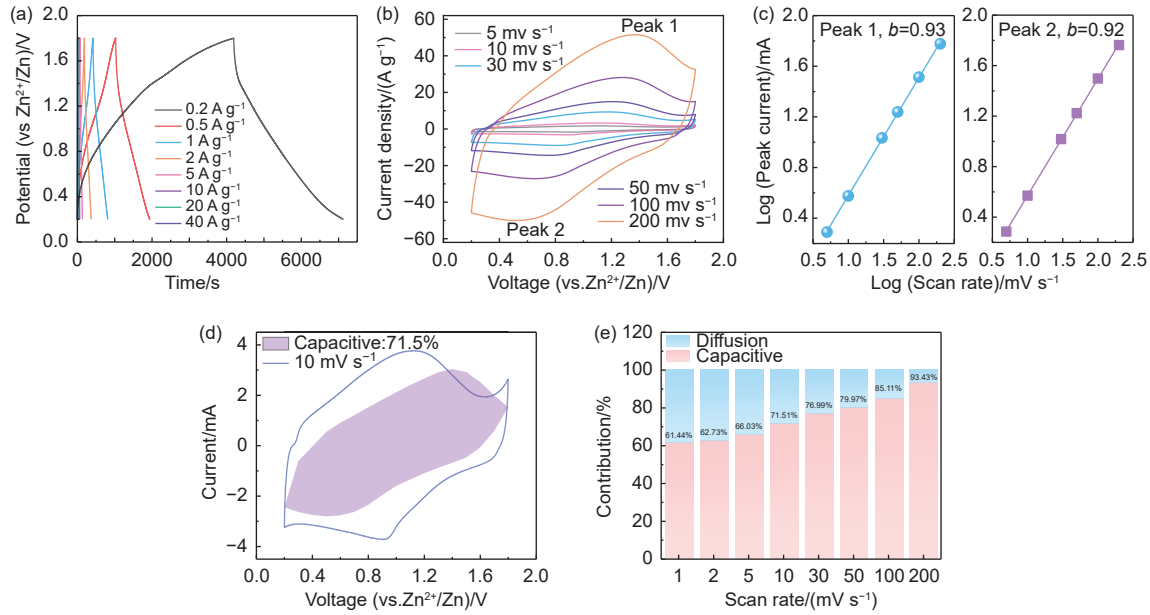

Fig. 5 (a) GCD curves at different current densities of NBSPC-4. (b) CV curves at different scan rates of NBSPC-4. (c) *b* values. (d) Capacitive and diffusion-controlled contribution to Zn storage of NBSPC-4 at 10 mV s^{-1}. (e) Normalized contribution ratio of capacitive and diffusion-controlled capacities at different scan rates

the scanning speed increases, the proportion of capacitance gradually increases[31,32].

4 Conclusion

In this work, the N, B co-doped sodium alginate-based porous carbon (NBSPC) has been successfully synthesized. The electrochemical properties of raw materials can be well improved through this efficient doping strategy of N and B. This N, B co-doped strategy can improve the materials wettability and electric double layer electrochemical behavior. When used as the cathode in zinc-ion hybrid capacitor (ZIHCs), NBSPC shows excellent rate performance (85.4 mA h g^{-1} even at ultra-high current density of 40 A g^{-1}) and cycling stability (15 000 cycles at 20 A g^{-1} with a capacity retention rate of 94.5%). This efficient strategy provides a new idea for developing high-performance ZIHCs cathode.

Declaration of competing interest

The authors declare that they have no known competing financial interests or personal relationships that could have appeared to influence the work reported in this paper.

Data availability statement

The data that support the findings of this study are openly available in Science Data Bank at https://cstr.cn/31253.11.sciencedb.j00125.00016 and https://doi.org/10.57760/sciencedb.j00125.00016.

Acknowledgements

This work was supported by the National Natural Science Foundation of China (52372039).

References

[1] Wang D, Zhang J, Li X, et al. Woven microsphere architected by carbon nanotubes as high-performance potassium ion batteries anodes[J]. Chemical Engineering Journal, 2022, 429: 132272.

[2] Liu L, Lu Y, Qiu D, et al. Sodium alginate-derived porous carbon: Self-template carbonization mechanism and application in capacitive energy storage[J]. Journal of Colloid and Interface Science, 2022, 620: 284-292.

[3] Lu Y, Liu L, Zhang R, et al. Sodium alginate-derived micropore dominated carbon 3D architectures through dual template engineering for high-performance Zn-ion hybrid capacitors[J]. Applied Surface Science, 2022, 604: 154631.

[4] Liu L, Du B, Liu R, et al. N-Doped hierarchically porous carbon aerogels by controlling the Zn –chitosan complex ratio for high-performance supercapacitors[J]. Energy & Fuels, 2022, 36(11): 5920-5927.

[5] Liu L, Sun X, Dong Y, et al. N-doped hierarchical porous hollow carbon spheres with multi-cavities for high performance Na-ion storage[J]. Journal of Power Sources, 2021, 506: 230170.

[6] Ding Y, Qi G, Cui Q, et al. High-Performance multifunctional structural supercapacitors based on in situ and ex situ activated-carbon-coated carbon fiber electrodes[J]. Energy & Fuels, 2022, 36(4): 2171-2178.

[7] Liu; L, Li; Y, Wang S, et al. High Sulfur-doped hollow carbon sphere with multicavity for high-performance Potassium-ion hybrid capacitors[J]. Journal of Colloid and Interface Science, 2022, 628: 975-983.

[8] Wang G, Li M, Zhang J, et al. Flexible, stable and durable polydopamine@lead zirconate titanate/polyimide composite membranes for piezoelectric pressure sensors and limb motion monitoring[J]. Composites Part C: Open Access, 2022, 8: 100292.

[9] Liu L, Sun Z, Lu Y, et al. d-Calcium pantothenate-derived porous carbon: carbonization mechanism and application in aqueous Zn-ion hybrid capacitors[J]. Journal of Materials Chemistry A, 2023, 11: 14311-14319.

[10] Liu L, Lu Y, Wang S, et al. B, N Stabilization effect on multicavity carbon microspheres for boosting durable and fast potassium-ion storage[J]. Journal of Colloid and Interface Science, 2022, 620(15): 24-34.

[11] Zhang P, Li Y, Wang G, et al. Zn-Ion hybrid micro-supercapacitors with ultrahigh areal energy density and long-term durability[J]. Adv Mater, 2019, 31(3): e1806005.

[12] Liu P, Fan X, Ouyang B, et al. A Zn ion hybrid capacitor with enhanced energy density for anode-free[J]. Journal of Power Sources, 2022, 518: 230740.

[13] Li H, Wu J, Wang L, et al. A zinc ion hybrid capacitor based on sharpened pencil-like hierarchically porous carbon derived from metal –organic framework[J]. Chemical Engineering Journal, 2022, 428: 131071.

[14] Shang P, Liu M, Mei Y, et al. Urea-Mediated monoliths made of nitrogen-enriched mesoporous carbon nanosheets for high-performance aqueous zinc ion hybrid capacitors [J]. Small, 2022: e2108057.

[15] Zhang Y, Wang Z, Li D, et al. Ultrathin carbon nanosheets for highly efficient capacitive K-ion and Zn-ion storage[J]. Journal of Materials Chemistry A, 2020, 8(43): 22874-22885.

[16] Yang L, He X, Wei Y, et al. Synthesis of N/P co-doped monolithic hierarchical porous carbon for zinc-ion hybrid capacitors with boosted energy density in $ZnSO_4/ZnI_2$ redox electrolyte[J]. Journal of Power Sources, 2022, 542: 231743.

[17] Li J, Yu L, Wang W, et al. Sulfur incorporation modulated absorption kinetics and electron transfer behavior for nitrogen rich porous carbon nanotubes endows superior aqueous Zinc ion storage capability[J]. Journal of Materials Chemistry A, 2022, 10(17): 9355-9362.

[18] Wu Z, Ye F, Liu Q, et al. Simultaneous incorporation of V and Mn

element into polyanionic NASICON for high energy-density and long-lifespan Zn-ion storage[J]. Advanced Energy Materials, 2022, 12: 2200654.

[19] Wang Y, Yang J, Liu S, et al. 3D graphene-like oxygen and sulfur-doped porous carbon nanosheets with multilevel ion channels for high-performance aqueous Zn-ion storage[J]. Carbon, 2023, 201: 624-632.

[20] Tang H, Yao J, Zhu Y. Recent Developments and future prospects for Zinc-ion hybrid capacitors: a review[J]. Advanced Energy Materials, 2021, 11(14): 2003994.

[21] Leng C, Fedossedva Y V, Zhao Z, et al. Rational-design heteroatom-doped cathode and ion modulation layer modified Zn anode for ultrafast zinc-ion hybrid capacitors with simultaneous high power and energy densities[J]. Journal of Power Sources, 2022, 536: 231484.

[22] Huang Z, Chen A, Mo F, et al. Phosphorene as cathode material for high-voltage, anti-self-discharge zinc ion hybrid capacitors [J]. Advanced Energy Materials, 2020, 10(24).

[23] Han L, Zhang X, Li J, et al. Enhanced energy storage of aqueous zinc-carbon hybrid supercapacitors via employing alkaline medium and B, N dual doped carbon cathode[J]. Journal of Colloid and Interface Science, 2021, 599: 556-565.

[24] Liu M, Zhu F, Cao W, et al. Multifunctional sulfate-assistant synthesis of seaweed-like N, S-doped carbons as high-performance anodes for K-ion capacitors[J]. Journal of Materials Chemistry A, 2022, 10(17): 9612-9620.

[25] Zhou C, Wang D, Li A, et al. Three-dimensional porous carbon doped with N, O and P heteroatoms as high-performance anode materials for sodium ion batteries[J]. Chemical Engineering Journal, 2020, 380: 122457.

[26] Zhuang R, Dong Y, Li D, et al. Polyaniline-mediated coupling of Mn_3O_4 nanoparticles on activated carbon for high-performance asymmetric supercapacitors[J]. ACS Applied Materials & Inter Faces, 2021, 851: 156871.

[27] Fan C, Dong Y, Liu Y, et al. Mesopore-dominated hollow carbon nanoparticles prepared by simple air oxidation of carbon black for high mass loading supercapacitors[J]. Carbon, 2020, 160: 328-334.

[28] Zhou C, Chen X, Liu H, et al. Heteroatom-doped multilocular carbon nanospheres with high surface utilization and excellent rate capability as electrode material for supercapacitors[J]. Electrochimica Acta, 2017, 236: 53-60.

[29] Qiu D, Gao A, Xie Z, et al. Homologous hierarchical porous hollow carbon spheres anode and bowls cathode enabling high-energy sodium-ion hybrid capacitors[J]. ACS Applied Materials & Inter faces, 2018, 10(51): 44483-44493.

[30] Qiu D, Li M, Kang C, et al. Cucurbit [6] uril-derived sub-4 nm pores-dominated hierarchical porous carbon for supercapacitors: operating voltage expansion and pore size matching[J]. Small, 2020, 16(29): 2002718.

[31] Chen G, Jiang Z, Li A, et al. Cu-based MOF-derived porous carbon with highly efficient photothermal conversion performance for solar steam evaporation[J]. Journal of Materials Chemistry A, 2021, 9(31): 16805-16813.

[32] Chen Y, Shi L, Guo S, et al. A general strategy towards carbon nanosheets from triblock polymers as high-rate anode materials for lithium and sodium ion batteries[J]. Journal of Materials Chemistry A, 2017, 5(37): 19866-19874.